Contents lists available at ScienceDirect

Carbon

journal homepage: www.elsevier.com

Interface graphitization of carbon-carbon composites by nanoindentation

Ahmed Sameer Khan Mohammed [a], Huseyin Sehitoglu [a,], Richard Rateick [b]

[a] Department of Mechanical Science and Engineering, University of Illinois at Urbana-Champaign, 1206 W. Green St., Urbana, IL, 61801, USA
[b] Honeywell Aerospace, 3520 Westmoor St., South Bend, IN, 46628, USA

ARTICLE INFO

Article history:
Received 28 January 2019
Received in revised form 10 May 2019
Accepted 15 May 2019
Available online xxx

ABSTRACT

The present study explores mechanical behavior of carbon-carbon composites using low-load nanoindentation. Indentations are performed using flat-punch and Berkovich tips indenting normal to the cross-section of a single fiber-matrix filament. A systematic set of tests are carried out employing multiple load functions to critically assess loading behavior and load-unload irreversibility at the filament scale. Flat-punch indentation response clearly shows irrecoverable displacements and an energy loss, accumulating over multiple cycles. This is compared against the indentation response of single crystal Aluminum where the unload-reload behavior is linear-elastic. The mechanical test is coupled with Raman micro-spectroscopy to correlate energy dissipation with structural changes in the carbon constituents. Three microstructurally distinct regions are identified using the Raman microprobe. First order spectra were tracked close to the interface revealing a reduction in the width of the defect peak. Constraining the nanoindentation footprint via a sharp-Berkovich indentation, the same correlation was confirmed. An incremental load-unload response was analyzed using the Oliver-Pharr model to reveal a consistent drop in indentation modulus with increasing maximum load. All observations suggest that graphitization could be the possible mechanism of plastic deformation in the material. The implications are discussed in relevance to toughness in structural and tribological applications.

1. Introduction

Carbon Carbon composites (abbreviated as C/C henceforth) form a special subset of carbon-fiber composites where the presence of an all-carbon system enriches expected properties of high specific stiffness, strength and toughness with exceptional thermal stability at high temperatures. These attributes in combination with high thermal conductivity, high specific heat capacity, low thermal expansion coefficient, high impact resistance, high ablation and wear resistance make these materials ideal candidates for applications involving severe conditions [1,2]. In that regard, these materials are prominent in advanced space and aircraft applications such as thermal protection barriers for atmospheric re-entry, rocket nozzles, exit cones and aircraft brake discs. Additionally, the biocompatibility and chemical inertness of elemental carbon has found use for this class of materials in the biomedical industry, for instance in fracture supporting plates, hip-joint prosthetics etc. [3,4].

The choice of an all-carbon system places carbon composites in the class of ceramic-matrix materials [5] (albeit with some differences [6]). In this class, the strength of the fiber-matrix interface plays a central role in determining fracture toughness, in both monotonic fracture and fatigue [7]. Any inelastic behavior (often termed pseudo-plastic) in tensile or shear stress-strain response manifests as a result of micro-fracture processes such as matrix cracking, interface cracking, fiber-bridging and pullout [8 10]. C/C materials, particularly those with woven fiber architectures, can exhibit good fracture toughness (an order higher than monolithic ceramics) [11] and fatigue tolerance [12] and much of it is attributed to the role played by these mechanisms in the crack wake zone. The importance of an optimal interface strength was highlighted in multiple studies [13 16]. In fatigue, flexure and tensile fatigue experiments had established a change in residual strength in high-cycle fatigue, dependent on the maximum applied stress, applied stress ratio and fatigue life [17 22]. Fatigue-induced interface fracture is established as the primary reason behind such effects, recent evidence of which is provided by techniques like Digital Image Correlation [23].

Furthermore, specific to C/C systems, relevance to tribological performance must be considered since it is the dominant commercial market for these materials [4]. The wear and frictional behavior are also dependent on the same pseudo-plastic and inelastic processes outlined previously. Tribological performance depends on the presence of a thin friction film (1 m) on the brake surface formed by the compaction of wear debris during the braking process [24 26]. Thus, the said processes govern the dynamic equilibrium prevailing between debris-generating fracture mechanisms, high-temperature oxidation loss and surface friction film formation. The fracture processes fundamentally depend on the interface bond strength and film formation attributed to the comminution of wear debris is contingent on plastic deformation of fiber and matrix phases [27 29].

In essence, the success of both structural and tribological responses rely on two basic properties: interface bond strength and inelastic dissipation in individual constituents. Multiple techniques have been developed to measure interface strength in brittle matrix

Corresponding author.
Email address: huseyin@illinois.edu (H. Sehitoglu)

https://doi.org/10.1016/j.carbon.2019.05.038
0008-6223/

systems [5] and applied to C/C materials [30 33]. Possibly the most convenient of these methods is a single fiber push out test, recently performed using flat-punch nanoindentation [34,35]. On the contrary, a systematic exploration of inelastic dissipation mechanisms has not been attempted, to the best of the author's knowledge. While sharp-tip nanoindentation (using Berkovich, Vickers, cube-corner indenters) has been used to infer matrix plasticity via a measure of hardness [36,37], the primary drawback is in the lack of understanding what the hardness means in relevance to turbostratic crystallite structures that constitute the composite. Possible prevalence of buckling mechanisms, complex deformation fields and appreciable variability questions the interpretation of results [38,39]. Moreover, the nature of the unload curve, whether it is elastic or has some reverse-plasticity, is yet unclear.

In this work, a coupled exploration of C/C inelastic behavior is attempted at the scale of a single fiber-matrix filament (refer Fig. 1). Flat-punch nanoindentation is used along with Raman micro-spectroscopy to connect energy dissipation with structural changes in both the fiber and the matrix. The choice of Raman spectroscopy was made for several reasons. One is the known sensitivity to low-energy structural defects [40] effectively covering the full range of crystalline states from amorphous carbon to crystalline graphite [41 43]. It has successfully served as a simple yet effective tool to rank the extent of quasi-crystallinity of different synthetic carbon materials, beyond just C/C systems [44 47]. Secondly, the technique is easy to perform and allows non-contact non-destructive monitoring of structural changes before and after a mechanical test. And lastly, the sampling spots of Raman micro-spectroscopes are well improved to diameters within 1 m, appropriate to characterize heterogeneous composite cross sections [48] while matching the scale of nanoindentation's spatial footprint. Berkovich indentations are also performed to provide supporting evidence corroborating the findings. It must be mentioned that a similar experimental coupling was carried out in Ref. [49] where carbon fibers were treated as strain sensors in ductile polymer-matrix composites. However, the measurement required a calibrating setup and primarily focused on correlation of Raman frequency shifts caused by elastic straining of carbon fiber to composite stress/strain measures. An understanding of plasticity or irreversibility wasn't addressed especially at a scale where the role of the fiber and matrix can be partitioned.

The goal of this study is to narrow focus to a scale where the load-displacement response is a direct indicator of the inelastic behavior of the fiber, matrix and the interface. Treating the interface analogous to a monolithic material, the motivation is to establish if there is an alternate intrinsic toughening mode which would impact friction film formation, monotonic crack growth resistance and also bring to the fore cyclic-inelastic effects involved in fatigue crack nucleation.

2. Methodology

2.1. Materials

The C/C specimens in this study were obtained from commercial aircraft brake discs, courtesy of Honeywell Aerospace. The fiber architecture constituted a needle-punched non-woven structure consisting of polyacrylonitrile (PAN)-based carbon fibers and low-temperature chemical vapor infiltrated (CVI) carbon matrix. The final composite was subject to graphitization heat treatment in an inert atmosphere. A diamond wafering blade mounted on a milling machine arbor was used to slice thin specimens of dimensions $15 \times 15 \times 0.5$ mm. The orientation was chosen so that a large number of fibers were oriented perpendicular to the specimen's indent plane (Fig. 1). The average diameter of the fibers was 8 m.

2.2. Experiments

2.2.1. Sample preparation

For structural characterization, samples were embedded in epoxy and polished, first using SiC papers (320 to P4000 grit) and then Alumina slurries (1 m to 0.05 m). Since the material is brittle and susceptible to abrasion-induced fracture, care was taken to have generous flow of lubricant (in this case, water) while applying minimal

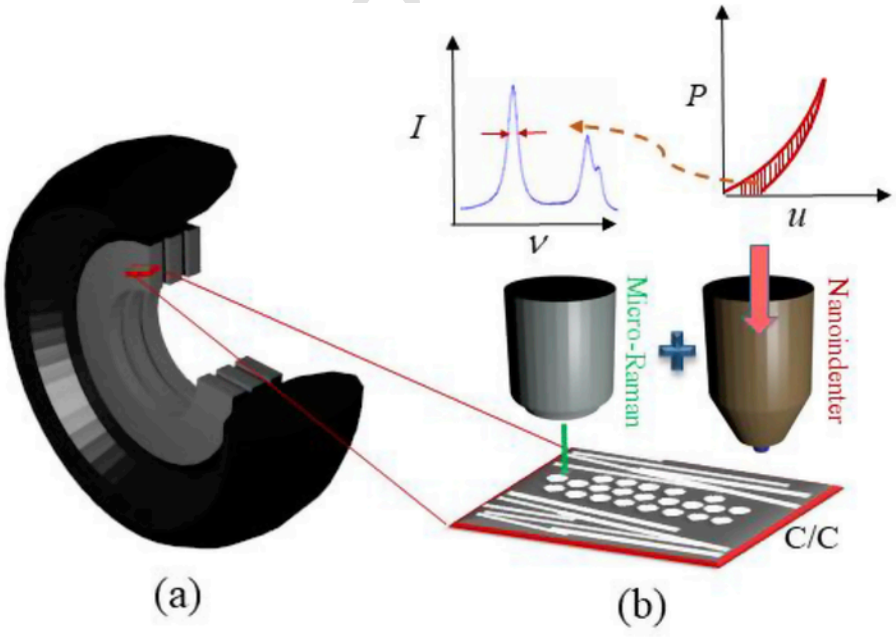

Fig. 1. (a) Schematic of carbon/carbon stator/rotor brake discs within aircraft landing wheels (b) Illustration of the coupled exploration using Nanoindentation and Raman Micro-Spectroscopy (RMS) aimed at connecting structural changes to dissipated energy in sample.

pressure just sufficient to hold the sample in place. For nanoindentation, samples were polished without the aid of any mount over diamond lapping films of grit sizes 6, 3, 1 and 0.1 m.

2.2.2. Structural characterization

The CVI-microstructure was characterized using Polarized Light Microscopy (PLM) [50,51] and micro-Raman spectroscopy [41].

Polarized Light Microscopy (PLM) was carried out in an optical microscope (Olympus BX51 M) with a polarizer, rotatable analyzer and a CCD having pixel resolution of 1600 × 1200. Images were collected at intervals of 1°. The sequence was analyzed in ImageJ [52], tracking a reference pixel point having maximum intensity in the crossed-polar configuration. The intensity curve is plotted for this pixel as a function of the analyzer angle to obtain the extinction angle curve. A second-order polynomial was chosen to fit the data motivated by the analytical form derived in Ref. [53].

The first-order Raman spectra were obtained on a HORIBA LabRAM HR Raman Confocal Imaging Microscope. The laser source was chosen to be of 532 nm wavelength, source power around 50 mW and incident polarization chosen along the preferred textural orientation of basal planes. For maximum resolution, grating density of 1800 gr/mm was chosen, and spectra was collected over a wide window of wavenumbers spanning 800 to 2000 cm^{-1} to have a reliable noise floor estimate. The objective had a magnification of 100× allowing a structural probe of 1 m size. A five-band spectral fitting procedure was employed following [41], performed using LabSpec 5. For structural characterization, five fiber-matrix cross-sections were analyzed. Sites were chosen in the web-region of the sample because the local structure is more representative of the deposition and heat treatment conditions and relatively independent of the surface area-to-volume ratio and hence also the local fiber volume fraction. At each site three locations are chosen, one in the CVI matrix (closest to the interface), second in the skin of the fiber [54,55], and the third in the central core of the fiber.

A five-band fitting procedure should ideally allow a characterization based on peaks and frequencies of five different peaks. However, only the measure of the full-width at half-maximum (FWHM) of the defect peak (D peak) is chosen as a marker for the structural state. It is the only peak in that wavenumber range that can be deconvoluted easily. The G-peak deconvolution is affected by the presence of the secondary defect peaks (*D*',*D*") and the relative intensity of the minor I-peak is low, close to the noise floor (refer Fig. 3).

2.2.3. Nanoindentation

Nanoindentation was performed at room temperature on the Hysitron Triboindenter TI 950®. At select sites, carbon fibers were indented normally using a 60° conical punch having a 5 m diameter circular flat end. The sites were picked from the web region where the local matrix volume fraction is the highest. This choice was motivated by the hypothesis that the soft-CVI matrix would play the primary role in bearing any plastic deformation. Since the study is focused on finding evidence of behavior that can be reliably resolved, sites showing a higher propensity for the same are preferred.

There are two motivating reasons behind the choice of a flat tip for nanoindentation. First is its popularity in interface characterization tests in composites. The stress field introduced by flat-punch contact has been studied analytically and computationally [56]. From these studies, it is known that the induced deformation is shear-dominated near the edges of the contact zone and the peak is achieved at a sub-surface point. In that regard, there is a better understanding of the nature of deformation induced by the indenter, as compared to sharper tips. In composite systems, particularly ones with appreciable elastic modulus mismatch, the shear-dominant loading of the interface is accentuated. Hence, it is reasonable to presume that the fiber-matrix interface is under shear loading. The dimensions are also chosen in accordance with the desirable stress-fields at the interface. A 5 m punch is chosen, lesser than the average fiber diameter. In this way, the interface zone is free from surface tractions and is primarily acted upon by interfacial shear stress. Now, consider this in relation to the preferred orientation of CVI crystallites. The applied shear primarily acts along the basal plane of crystallites shearing them in their most compliant mode and possibly activating inelastic deformation mechanisms. This hypothesis draws on the ease of basal plane dislocation slip in single-crystal graphite [57] and also on early tests performed on monolithic high-temperature pyrocarbons [58,59]. These tests were performed at high-temperatures where vacancy diffusion was dominant. At room temperatures however, it may be possible that a plastic slip-like mechanism is active, similar to the classical picture of graphitization that was thought to involve movement of whole layer planes [60].

Secondly, the prevalence of a constant area of contact on the sample simplifies behavior of the load-displacement curve. Any material exhibiting an elasto-plastic response (time-independent plasticity) would exhibit a load-displacement response similar to uniaxial stress-strain response in a tensile testing machine [56]. There would be a stiff regime dominated by elastic response and a compliant flow regime dominated by plasticity. This is confirmed by testing a standard sample, single crystal Aluminum having [1 0 0] orientation aligned with the indentation axis. Any nonlinearities due to a changing contact area is eliminated facilitating identification of the onset of plastic flow. Nevertheless, it must be mentioned that a perfectly elastic regime is hard to obtain in the loading curve. This is primarily because of limited scale plasticity introduced at tip corners, and also because of time-dependent effects in low-load nanoindentation. On the other hand, the unload curve definitely shows recoverable linear-elastic behavior, a fact used in nanoindentation models in the guise of the flat-punch approximation [58]. Hence, linearity of response can be expected in the unload curve, an absence of which is definite indication of inelastic behavior.

The composite sample was gripped on the magnetic stage of the nanoindenter using small microscope stage-clips. The use of a secondary mount (e.g. AFM disc) with cyanoacrylate/crystal bond wax was avoided because the sample's high stiffness in tandem with a blunt indenter (flat-punch) exacerbated the creeping response of the adhesive.

With the flat-punch, two types of loading functions were chosen: Single load-unload, two-cycle load-unload at varying R-ratios ($R = \frac{P_{\min}}{P_{\max}}$, where $P_{\min}$ and $P_{\max}$ represent the minimum and maximum nanoindenter loads applied in the second cycle, respectively). Each loading function is chosen to highlight different aspects of mechanical behavior. The single load-unload function is used to probe typical pre-fracture behavior at different loads. Since the area of contact will be a constant, the loading curve will be expected to show a linear response unless there are some inelastic effects involved. The two-cycle load-unload function will be used to check if the unload curve is elastic, commonly presumed in nanoindentation measurements.

Indentations were performed at low loads (within 10 mN), under load control at constant loading rate of 0.5 mN/s. The maximum load of indent is chosen to ensure that pre-fracture behavior is probed and no interface debond is initiated. A safe value is arrived at by performing multiple indents locally. Typically, any initiation of interface debond reflects as an abrupt transition in the slope of the load-displacement curve [34]. The loading curves are checked for this transi-

tion, and high-magnification optical micrographs (100×) are compared before and after test to ensure no cracks are formed (revealed by a thin dark outline around the fiber).

An important challenge in nanoindentation is the issue of variability [61] depending on choice of indent location. Particularly in C/C systems, the indentation response at each location can be influenced by the extent of local porosity, local textural variations of the CVI deposits or presence of micro-cracks in the matrix. These can affect certain characteristics of the load-displacement response such as the maximum depth of indent at peak load, or the stiffness of loading response etc. Typically a large number of sites are averaged over to get representative load-displacement curves. On the contrary, the focus here is not on obtaining a representative load-displacement curve for the sample but more toward establishing the behavior in the material. To that extent, the results presented are from a select number of individual tests and not averaged.

Supplementary to the flat-punch indents, standard Berkovich-tip indents are also performed on carbon fibers normal to the cross section. The purpose of the Berkovich indent is many-fold. It allows comparison with response of a popular calibration sample, fused quartz. The deformation zone is localized to a small region, much smaller than the flat-punch's footprint. This allows the indentation response of the fiber and the CVI matrix to be probed independently. An incremental load-unload function is chosen to compare the indentation response of CVI and fiber against that of fused quartz. The unload curves at each incremental cycle are analyzed using the Oliver-Pharr model [62]. In this model, a power-law fit of the unload curve is used to extract the contact depth at each cycle's maximum load, allowing a measure of indenter contact area and consequently the indentation moduli. It must be emphasized the indentation modulus is different from the elastic modulus measured in tension/compression, as has been shown in recent indentation studies on carbon fibers [63 67]. Lastly, the sharp Berkovich tip (tip radius within 100 nm) can be used to perform imaging using Scanning Probe Microscopy (SPM). The surface can be scanned for residual deformation which can otherwise be difficult to spot using optical/electron microscopy. This is because the penetration depths are low at the chosen applied loads and because the C/C components exhibit a high level of recovery [38]. As an additional check, a surface scan is used to measure the surface roughness, an important measure to ensure that the observed low-load response is not caused by partial contact at surface asperities.

2.2.4. Nanoindentation with ex situ Raman characterization

RMS was also used to track structural signatures before and after nanoindentation. The Raman optics included an analyzer parallel to the incident polarization direction. This was done to selectively emphasize structural changes in preferentially oriented crystallites [52]. Optical microscopes on each instrument ensures that the indentation is performed at the site characterized by Raman spectra. However, to track structural changes it must be ensured that the same spot (1 m size) is probed before and after nanoindentation. If not, a case of mistaken identity results where the sampled spot after test may not be the same one probed before the test. No reliable trend may be observed because the spectral changes will be marred by spatial variability of Raman spectra in the same sample. The HORIBA LabRAM HR has a motorized stage allowing positioning to the nearest micron. Nevertheless, there is significant backlash at the start and stop of motor movements causing offsets of the order of half micron. There are also errors associated with angular misalignments of the sample's preferred basal plane orientation with the incident polarization. By fixing an origin reference on physical features visible next to each site and keeping the relative X Y positions of the sampled spot consistent within 1 m, both positioning and alignment errors are eliminated to a large extent. To make the measurement more robust, multiple spots are probed at each target location. A tradeoff is apparent here. Sampling of multiple spots increases the likelihood of probing the same location in an average sense. But this comes at a cost of loss in sensitivity of measurement because local structural gradients [38,48] will cause scatter and obscure the trends.

With flat-punch indents, structural signatures are tracked in the CVI matrix and fiber skin close to the interface. Two cycles of a 5 mN indent are applied with intermittent Raman characterization at these locations. As additional evidence, the experiment is repeated on a Berkovich indent in the fiber. The fiber is chosen as the site of indent because of transverse isotropy in its structure. If the CVI is chosen, there could be additional artifacts introduced by the orientation of the Berkovich tip with respect to the preferred texture. A benefit of choosing the Berkovich indent is that it causes a localized deformation zone which can be sufficiently covered by the micron-sized RMS laser spots. In a sense, it allows a more direct correlation between the energy loss and spectra changes in a confined region.

3. Results

3.1. Structure

An optical micrograph of the composite cross-section viewed under crossed-polars is shown in Fig. 2 (a). The reference pixel that was tracked is indicated. The extinction angle was determined from the position of the minimum of the curve plotted in Fig. 2(b). The value is found to be approximately 17°. Results of Raman characterization

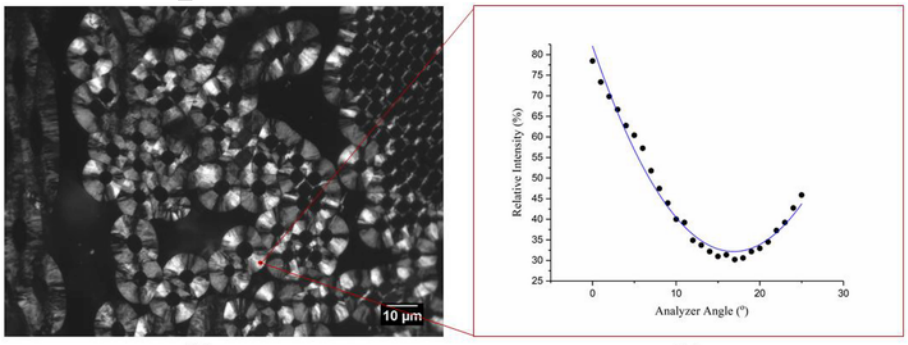

Fig. 2. (a) C/C cross-section viewed under crossed polars (b) Extinction angle curve plotted by tracking a reference pixel in the PLM micrograph.

are shown in Fig. 3. The $FWHM_D$ values of the fiber core, skin and the CVI are tabulated in Table 1. There is a clear difference in structural signatures in each of these regions.

3.2. Nanoindentation: flat-punch and Berkovich indents

Typical pre-fracture indent behavior of C/C is shown in Fig. 4. Test results are shown at two representative loads of 5 mN and 10 mN. It must be mentioned that this behavior was observed at loads as low as 100 N. The loading curve seems linear with no evident signs of a transition from an elastic to a plastic regime. Since the unload curve did not retrace the loading curve, there are definite inelastic effects involved. Going by the hypothesis that the sample shows time-independent plastic mechanisms, one would expect the unload curve to be completely elastic and linear. On the contrary, the unloading curve shows a high nonlinearity indicative of some reverse-plasticity or other unknown inelastic effects. It is possible that a part of the unload curve is elastic and there was an onset of reverse-plasticity at some point. The incremental test on Al [1 0 0] serves as a reference standard for elasto-plastic response (Fig. 5). The envelope of the response resembles the stress-strain response of ductile single crystals with a distinct flow regime [56]. The unload-reload segments at different stages retrace perfectly, implying a perfectly elastic unload.

To check for reverse plasticity in C/C, a two-cycle indent was performed, at two different R-ratios. A lower R-ratio was chosen at a higher load of indent to exemplify any hysteresis. A higher R-ratio was chosen at a lower-load to check for possible elasticity at low loads. The results are shown as inset plots in Fig. 4. It is clear that the unload curve is not elastic and there is a hysteresis in the response. At a higher R-ratio, the reload curve tends to approach the unload curve and there seems to be a retraceable near-elastic region.

The results of Berkovich indents performed on standard sample Quartz are presented in Fig. 6 (a). The non-linearity of the loading curve is primarily because of elasto-plastic deformation under a changing area of contact. Note that the unload curves are clearly elastic because they are perfectly retraced upon reload. The apparent increase in slope of the unload curve should come as no surprise because the contact area of the indenter is also increasing. However, the estimated indentation modulus is expected to stay constant. Any increase/decrease is indicative of possible structural change causing the sample to become more stiff/compliant respectively. The Oliver-Pharr model is adopted to infer the indentation modulus from the unload curve. The tip-area function is calibrated on the Quartz sample because it is known to have lesser time-dependent effects and reproducible properties irrespective of the depth of indent [61]. The indentation response of the CVI matrix and the carbon fiber are shown in Fig. 6 (b) and 6 (c) respectively. Note that the inelastic dissipation is higher in the CVI than the carbon fiber. The unload curves are not elastic. Nevertheless, following the result of low-R unload-reload behavior, the existence of a brief near-elastic regime is hypothesized. With this approximation, the Oliver-Pharr model is fit to the unload curve within 20% of the maximum load and the inferred moduli are compared. The results are shown in the insets. It is worthwhile to note that the trend doesn't change much when the analysis is repeated by fitting the entire unload curve. Both the CVI and the fiber show evidence of becoming more compliant.

3.3. Indentation and Raman spectroscopy

The change in Raman signatures before and after flat punch indentation are presented in Fig. 7. Significant spectral changes are observed in both the skin of the fiber and the CVI matrix. The width of the D-peak reduces. Additionally, a marginal decrease in G-peak width along with its frequency is also observed. Those results are not presented here for brevity, and also because of aforementioned complications associated with G-peak deconvolution. This observation has been consistently observed at 4 different fiber push sites. All the spectral changes correspond to an increase in crystalline perfection, tending towards a more graphitic structure [41,45,48]. In other words, the shear-loading of the interface has caused a local graphitization at the interface, causing the fiber skin and the CVI matrix to graphitize. Graphitization refers to the solid-state transformation of quasi-crystalline non-graphitic (or partially graphitic) carbon to crystalline graphite, so far known to occur under high-temperature heat treatment (1700 3000 centigrade) [68,69]. The work done by the nanoindenter has been absorbed in the form of energy for the graphi-

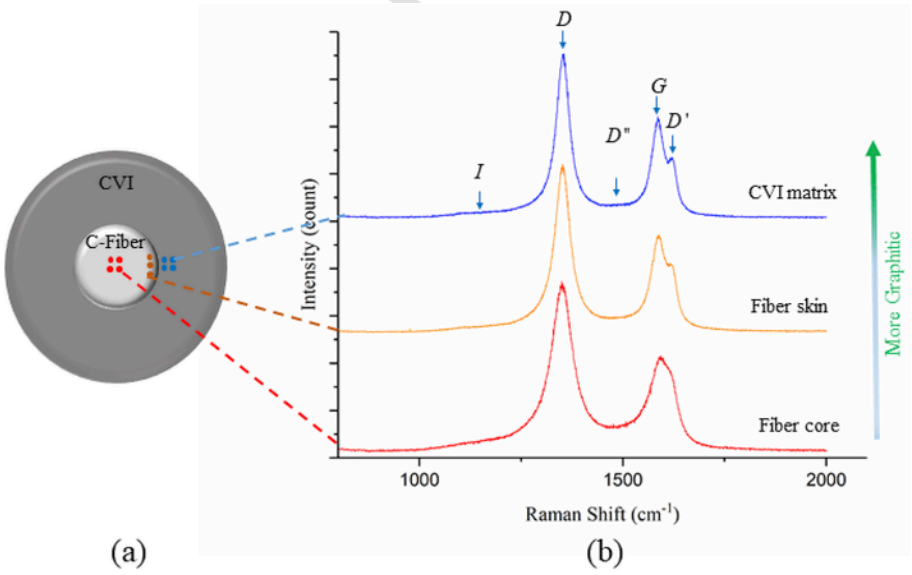

Fig. 3. (a) Schematic cross-section of a single fiber-matrix filament and sampling of multiple Raman spots in different regions (b) Typical spectra in the three microstructurally distinct regions, ranked from highest to lowest in terms of graphitic order (the relevant peaks are indicated).

Table 1
Width of defect peak (D) in Raman spectra.

Micro-constituent	$FWHM_D$ (cm^{-1})
CVI Matrix	46.63±2.30
Fiber Skin	48.18±2.71
Fiber Core	66.72±1.69

tization process. To check if this change accumulates in the form of cyclic inelasticity, the spectra changes with intermittent two-cycle indents are presented. The load-displacement data of a single-cycle is also presented concomitantly.

A validation of the observed spectral change was carried out using Berkovich indentation. The idea was to constrain the deformation zone and conclusively establish that there is a spectral change in that region that could have only been caused by the Berkovich indent. The results are presented in Fig. 8. Note that the indent was in the core of the fiber, and it has graphitized.

Two validation checks are carried out using the Berkovich tips. Firstly, the above indent mark is imaged to see if there is indeed an irrecoverable impression created on the sample, corresponding to the residual displacement in the load-displacement curve. The imaging is carried out in the SPM (Scanning Probe Microscopy) mode. The corresponding post-test surface scans are presented in Fig. 8. The scans are tilt corrected and plotted using Gwyddion [70]. The tilt angle was approximately 0.5°, which doesn't cause significant change in the response or inferred properties [71]. The impression resembles the behavior of a sample exhibiting high recovery. Additionally, the surface scans allow an estimate of roughness, which is found to be less than 1 nm. The check was to confirm that all depths of indents are atleast 5 times the roughness value to avoid errors caused by partial contact. Clearly, this condition is satisfied in all indents.

4. Discussion

Characterization using PLM provides a quick and effective way to classify C/C based on the textural arrangement of crystallites. The sample is found to be optically anisotropic with a relatively high extinction angle. According to the classification proposed in Ref. [51], the microstructure is one among Rough Laminar or Regenerative Laminar textures [72]. RMS analysis complements the inter-crystallite arrangement with intra-crystallite information. The width of the defect peak ($FWHM_D$) in the Raman spectrum serves as a useful parameter corresponding to that information. Following the structure-texture map proposed by Bourrat [52], it is clear that the microstructure is Rough Laminar (RL).

As mentioned previously, RMS is a convenient method to probe structure at a sub-micron scale. When used to characterize the fiber structure, it has revealed a distinct skin-core effect where the fiber skin is better ordered than the fiber core. This effect has been explored primarily using Transmission Electron Microscopy (TEM) [54]. The crux of these studies is that there is a fiber skin, not larger than 1 m in thickness where the turbostratic crystallites have better circumferential texture than in the core and are also aligned end-to-end along the length of the fiber. Hence, the information was still on a textural scale. The present study complements this observation with evidence from Raman spectra. The skin is indeed found to be more graphitic than the core, possibly having a higher propensity for slip-like behavior or for vacancy diffusion along basal planes.

The flat punch was chosen with the idea that the shear-dominated loading at the interface would cause a slip-like behavior in the preferentially oriented CVI matrix and also possibly the fiber skin. In such a scenario, a load-displacement response analogous to that of single crystal Aluminum was expected where there is a stiff elastic regime

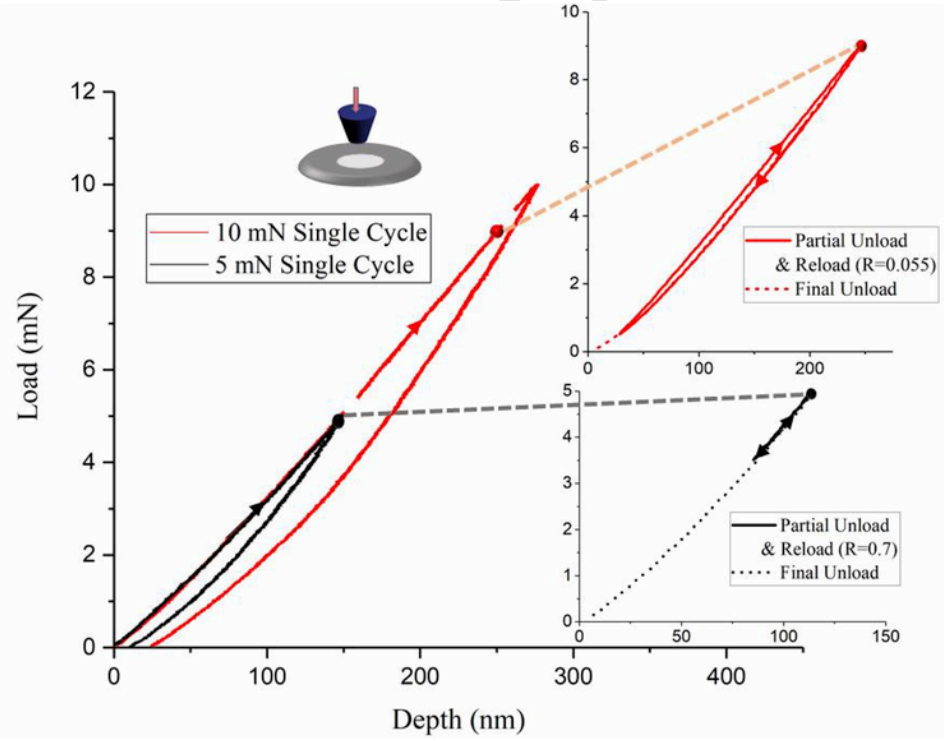

Fig. 4. Flat-punch indentation behavior of C/C before initiation of any interface debond. The inset plots show the unload-reload hysteresis from distinct maximum loads and R-ratios.

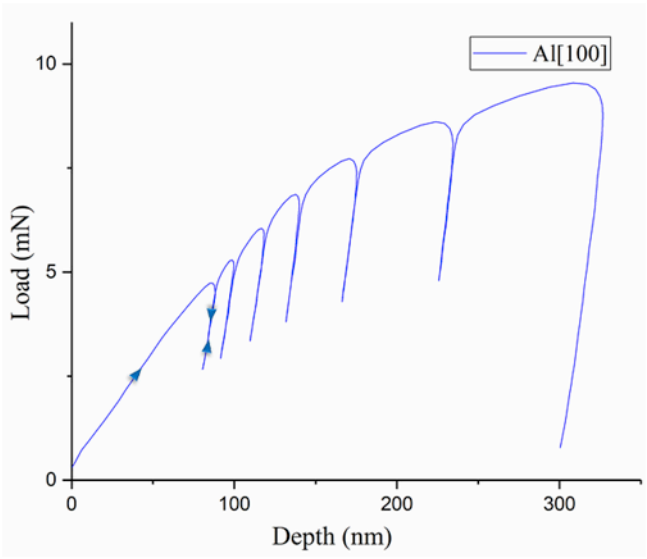

Fig. 5. Flat-punch indentation behavior on reference sample Al [100].

followed by a plastic flow regime. The unload curves were expected to be perfectly elastic allowing a complete retrace upon reload. However, none of these behaviors were exhibited by C/C. The flat punch indentation did seem to exhibit a deceptively linear loading response although its true nature is better understood as an increasingly stiffening curve, as explained in reference to other test results. The unload curve exhibits a highly non-linear trajectory which is not retraced by the reload curve. Hence, there is a clear pre-fracture inelastic response and energy dissipated in the sample. Incremental load response under Berkovich indents emphasized this inelasticity individually in the CVI and the fiber. The CVI seemed to exhibit a more pronounced energy dissipation capacity as compared to the fiber. An analysis using the Oliver-Pharr model reveals that the indentation modulus shows a consistent drop with an increase in the magnitude of unload. The reducing indentation moduli are reminiscent of the trend found in elastic characterization of C/C samples heat treated at different temperatures [39]. The study on heat-treatment had established that the graphitization induced by the heat-treatment correlated with a reducing indentation modulus. This was explained based on the increased susceptibility of graphitized crystallites to basal plane shear. It seems likely that a similar phenomenon may be underway here. There could be a mechanical graphitization occurring with the energy absorbed at each cycle. The fact that the CVI shows a higher hysteresis than the fiber is consistent with the commonly held notion that the matrix is more graphitizable in C/C materials. If the incremental response evidences a progressive graphitization at increased load magnitudes, then a similar process must be underway during flat-punch indentation. Since graphitization is associated with an increase in in-plane tensile/compressive elastic modulus, the loading response in flat-punch indentation must be non-linear possibly exhibiting a stiffening response.

The evidence of Raman spectra change provides conclusive evidence that the inelastic behavior is caused by graphitization of the sample. The CVI matrix and the fiber skin are both subject to this change exhibiting significant reductions in the spectral width parameters. The graphitization also explains the subtle stiffening behavior in the loading curve. The degree of structural perfection is increasing in the basal-planes, stiffening the indentation response at increasing loads. Although not established here, the magnitude of this increase would be highest closest to the interface and recede further away

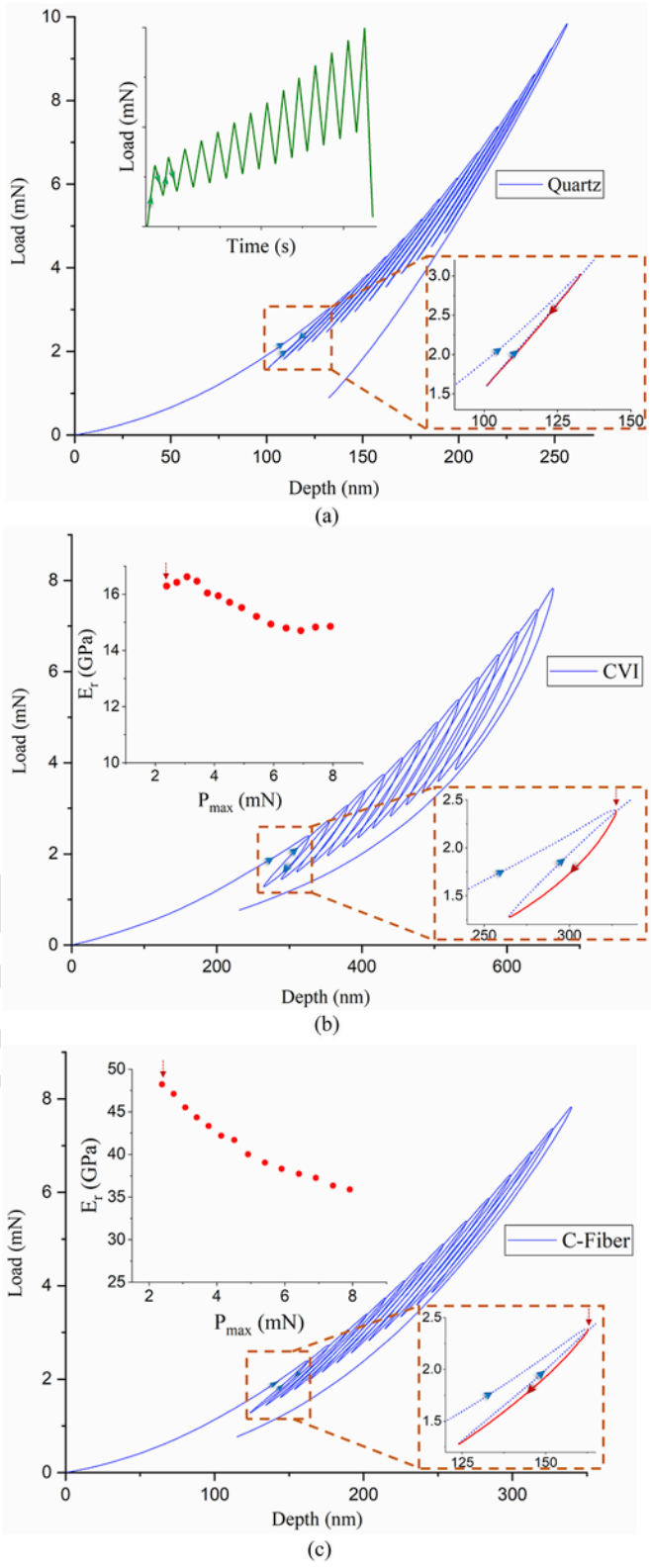

Fig. 6. (a) Incremental load-unload response of Quartz, left inset shows a schematic of the load function and the right insets plots a single unload-reload segment (b) Incremental response of CVI matrix and (c) fiber, left inset plots indentation moduli against magnitude of unload, the right inset shows the correspondence between one of the unload segments and associated data point in the indentation modulus plot.

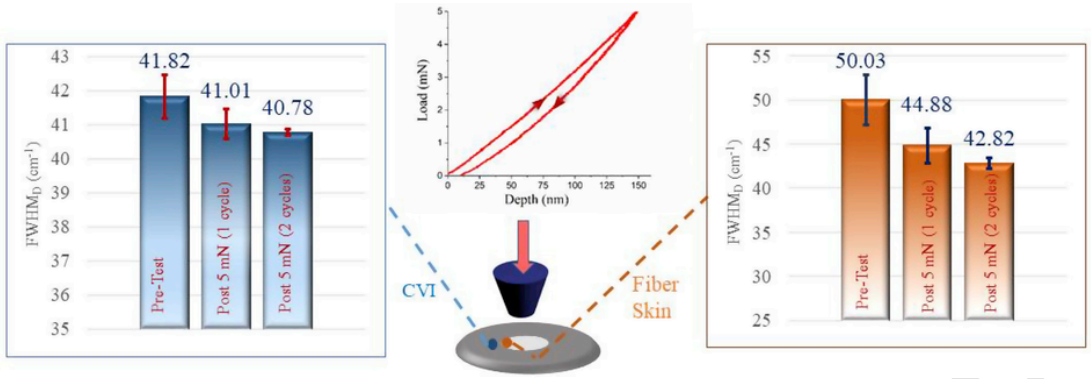

Fig. 7. Results of *ex situ* study with RMS and flat-punch nanoindentation: Defect peak width reduces with indentation (accumulates over multiple cycles).

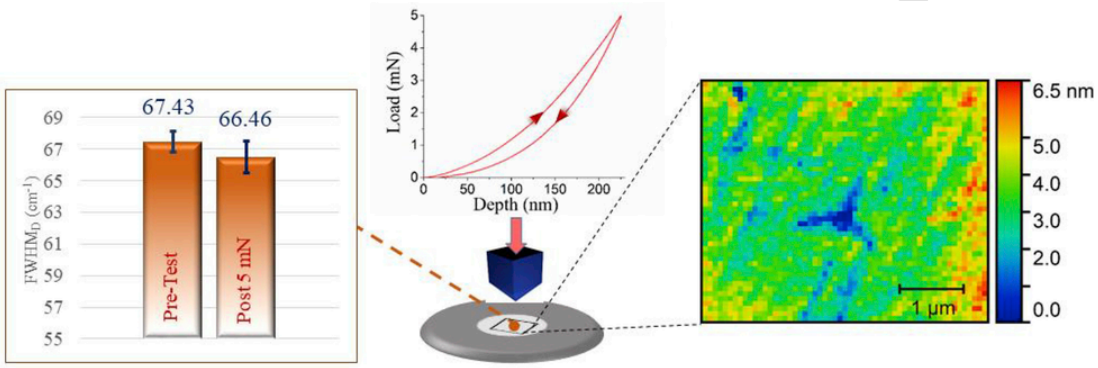

Fig. 8. Results of *ex situ* study with RMS and Berkovich nanoindentation: Defect peak width reduces with indentation. The indent is also imaged in the SPM mode.

from it, consistent with the magnitude of basal-plane-aligned shear stress at these locations. The open question that remains is the mechanism that brings about such change. If there was a slip-like behavior as was expected, then the indentation response would be quite different. The loading curve would have possibly shown an onset of plastic flow. The unload curve would have been linear elastic at least at higher R-ratios, as in the case of single crystal Aluminum. However, the response was more complicated. The unload-reload hysteresis does not seem to be eliminated at higher R-ratios, implying a possible absence of any elastic regime at all. There is an abrupt change in the slope of the curves, at the point of reversal from unload and reload. The extent of slope change depends on the magnitude of load at the reversal. Such a response is uncharacteristic of an elastic-time-independent-plastic response and indicative of a time-dependent behavior. Drawing on the studies of high-temperature creep deformation in pyrocarbons [59], it does not seem unreasonable there may be an in-plane vacancy diffusion even at room temperature. The high interfacial shear stresses may have provided the primary impetus in place of high temperatures. The tangential orientation of the graphitic crystallites at the interface (in the CVI matrix) facilitates the process because the applied shear acts along the basal planes. Vacancies diffuse along the basal planes within crystallites, annealing structural defects and making the structure more graphitic. Consistent with the time-dependent nature of diffusion mechanisms, the observed behavior might be more amenable to a framework incorporating viscous rate-dependence.

As mentioned before, the purpose of the Berkovich tip was to create a local deformed zone and directly connect spectral changes with dissipated energy in the load-displacement curve. In contrast with the flat-punch indents, the sampled RMS spots can fully cover the deformation zone and it is unlikely that anything other than the imposed mechanical test could have brought about the change in structural signatures. Consistent with the previous observations, the fiber core also exhibits a graphitization. This is particularly surprising in context of PAN-based carbon fibers because they are typically considered to be non-graphitizable under heat treatment. However, it must be remembered the fibers are not graphitizable to an appreciable extent to be measurable with X-Ray Diffraction (XRD) or TEM. The mechanical treatment here is caused by a special sharp tip on a small zone and the sensitivity of the instrument just happens to pick up the change. Since the reliability of the measurement rests on averaging over multiple spots, it is not possible to further resolve gradients in the degree of graphitization within the deformation zone. In this regard, it cannot be further specified if the region close to the tip periphery or that directly under the tip graphitizes the most. This approach establishes inelasticity in the PAN-fiber at room-temperature, contributing to previous studies in literature where inelasticity of carbon fibers has been established at high-temperatures [73 75]. For the sake of completion, it is justified to question occurrence of graphitization in the core of the fiber, when the flat-punch was employed instead of the Berkovich tip. The authors did not attempt a comparison of core spectra in this scenario and provide brief arguments that can guide future studies in this direction. A major challenge in obtaining a measurable spectral change could be the absence of sufficient stress magnitudes in the footprint of such blunt indenters, as compared to those induced by the sharp Berkovich tip. However, it is known that the stress-state under the flat punch has a high hydrostatic pressure component [56] which is known to promote graphitization [76]. Contrarily, there may also be a competing disordering effect from the compression of basal planes perpendicular to the *c*-axis of the crystallites [39]. The result-

ing spectra change may involve an interplay of these effects and must be addressed to establish graphitization of the core under flat-punch indentation.

C/C materials were known to exhibit graphitization at heat treatment temperature higher than 2000 centigrade [41]. The presented results indicate that there is local mechanical graphitization at the interface without any high-temperature heat treatment. The term mechanical is used in-place of stress-induced graphitization because the latter has been used to refer to the role of applied mechanical stress in facilitating the graphitization process [77]. In stress-induced graphitization, the presence of a thermal residual stresses at the interface was hypothesized to explain the anomalously higher graphitization of the C/C interface at high heat treatment temperatures [77 82]. While a causal link that determines the most favorable stress-state for graphitization mechanisms is still missing, experimental evidence of graphitization through microscopic/spectroscopic techniques and calculations of matrix-fiber thermal mismatch stresses have established, in a correlational sense, the deviatoric nature of the stress-state [83]. The proposition from the study is that there is a stress-induced graphitization prevalent even at room temperatures. It seems likely that under any load, the interface would be subjected to a similar deviatoric state, one of high basal-plane shear in this case, activating the mechanisms necessary to transform the structure.

The implications of such behavior can be quite fundamental in many applications. In tribological applications, the wear surface is subjected to high temperatures while sustaining braking pressure and frictional loads. It is likely that the wear debris generated from interface fracture has already undergone graphitization. The hardness of the wear debris is decided by this final graphitic state. Consequently, the hardness governs the ease of friction film formation through amorphization processes. In structural applications, the most direct relevance is to interface-fatigue. The graphitization of the skin and CVI matrix under cyclic loading can cause a change in the intrinsic interface strength. The textural arrangement of crystallites at the interface suggests that the interface strength would be dependent on the number of unsaturated out-of-plane bonds. As the crystalline perfection is increased, the out-of-plane bonding will reduce and only weak van der Waals forces would govern the strength. Hence, it seems likely that the interface graphitization could in fact weaken the interface over multiple cycles of loading. Nevertheless, it must be mentioned that the process could be more complex due to the presence of a semi-crystalline phase at the interface [29]. This nano-scale phase is optically not resolvable and hence not amenable to study by this method. It is worthwhile to note that the proposed interface graphitization could explain the observation of modified residual strength post high-cycle fatigue [22]. The effect is most likely a compromise between in-plane strengthening via graphitization and also interface cracking during fatigue. Furthermore, in terms of static interface strength, the graphitization process can have crucial bearing. With increased loading, interface graphitization may tend to change the interface strength by the same hypothesis presented previously. Simultaneously there is an increase in the elastic energy release rate because of the increase in in-plane tensile/compressive modulus associated with graphitization. The meeting point of the two trends would decide the interface strength, the single-most crucial parameter in impacting ceramic composite toughness.

In closing, it seems prudent to complement presented experimental evidence with a brief discussion on possible modeling approaches. Based on previous assessment of the indentation response, a time-dependent visco-elastic or visco-plastic model is deemed appropriate. The load-displacement data can be translated into continuum properties of storage elastic moduli and loss moduli, the latter of which quantifies the extent of toughening [61]. Material parameters extracted from Berkovich indentations are representative of individual constituents while those from the flat-punch indentations express the combined response. At the crystallographic scale, atomistic simulation techniques may provide insight into governing deformation mechanisms participating in interface graphitization. The shear-dominated loading at the continuum scale can be abstracted to a basal plane shear applied to a nanostructural model of turbostratic crystallites [84]. Molecular Dynamics (MD) simulations [85] under applied stress can be used to determine the operative mechanisms, possibly motion of dislocation-like elements [84] or simply vacancy diffusion. This would clarify, at a fundamental scale, how the atomic-scale movements accommodate inelastic deformation, and establish graphitization as a mechanism of inelastic deformation in C/Cs. The reliability of this approach rests on the performance of the underlying empirical interatomic potential and it is fortunate that a number of such potentials have been developed to capture carbon's versatile bonding nature ([86 88] to name a few). A more *ab initio* approach would be to compute energy barriers for the determined mechanisms using Density Functional Theory (DFT) [89]. At that scale, the propensity of graphitization may be modeled by exploring the dependence of the energy cost on the degree of crystallinity of the model structure. Such understanding at multiple scales would go much further than explaining C/C behavior and delve into mechanics of graphitization, pertinent to all pyrocarbon materials.

5. Conclusions

The presented study explores the mechanical behavior of carbon-carbon composites through nanoindentation, with special emphasis on inelastic energy dissipation within the material. The composite is tested using flat punch indentation to focus attention to the scale of a single fiber-matrix filament. It was revealed that nanoindentation response has some peculiarities unlike elasto-plastic indentation behavior of metals like Al [1 0 0]. These features are attributed to possible time-dependent viscoelastic or viscoplastic processes. The loading curve shows a subtle stiffening behavior while the unloading curve is highly nonlinear. The behavior was understood by an *ex situ* coupled study of flat-punch nanoindentation and Raman spectroscopy. It was found that the hysteretic energy loss causes a change in the Raman signature that is typically associated with graphitization of turbostratic structures. The graphitization was found in the CVI matrix and also in the fiber skin. Validating checks were performed using Berkovich indents on fibers and CVI matrix. The differences in the extent of hysteresis reiterates the well-known difference in graphitizabilities of the two constituents. The indentation modulus exhibits considerable reduction with increase in indentation load, also consistent with the presented hypothesis. Raman characterization at Berkovich-indented locations confirmed similar spectral trends. A surface scan was also performed to check for the residual impression and to invalidate possible complexities due to surface roughness.

The novelty of this study derives from the nexus of two techniques that have hitherto been employed independently. In what would be considered an atypical exploration for ceramic systems, an inelastic dissipation mechanism has been established which is intrinsic to the system and independent of any micro-fracture processes. To the best of the author's knowledge, this is the first study in C/C materials to conclusively establish the energy-absorbing behavior to be a direct consequence of graphitization. And contrary to the synonymous correlation of graphitization with high temperature treatment, this process is observed at room temperature, driven by mechanical stress. Finally, this study finds that the carbon fiber also plays a role

in composite toughening apart from acting as a stiff structural backbone. The fiber skin graphitizes similar to the CVI matrix, highlighting the fundamental structural similarity between fiber and matrix constituents in C/C systems. The implications of interface graphitization on the structural and tribological properties are discussed along with possible modeling approaches. Graphitization is the mechanism of inelastic energy dissipation and the propensity to graphitize in the fiber and the matrix can dictate composite properties.

Acknowledgements

We would like to thank Honeywell Aerospace for funding this study and for providing the composite specimens. The experiments were carried out partly in Frederick-Seitz Materials Research Laboratory (FSMRL) and Beckman Institute of Advanced Science and Technology at the University of Illinois.

References

[1] J.D. Buckley, D.D. Edie, Carbon-carbon Materials and Composites, vol. 1254, William Andrew, 1993.
[2] E. Fitzer, The future of carbon-carbon composites, Carbon 25 (2) (1987) 163–190.
[3] L.M. Manocha, E. Fitzer, Carbon Reinforcement and C/C Composites, Springer Berlin, 1998.
[4] E. Savage, Carbon-carbon Composites, Springer Science & Business Media, 2012.
[5] A.G. Evans, F.W. Zok, The physics and mechanics of fibre-reinforced brittle matrix composites, J. Mater. Sci. 29 (15) (1994) 3857–3896.
[6] K.R. Turner, J.S. Speck, A.G. Evans, Mechanisms of deformation and failure in carbon-matrix composites subject to tensile and shear loading, J. Am. Ceram. Soc. 78 (7) (1995) 1841–1848.
[7] A.G. Evans, F.W. Zok, J. Davis, The role of interfaces in fiber-reinforced brittle matrix composites, Compos. Sci. Technol. 42 (1 3) (1991) 3–24.
[8] R.Y. Kim, N.J. Pagano, Crack initiation in unidirectional brittle-matrix composites, J. Am. Ceram. Soc. 74 (5) (1991) 1082–1090.
[9] L.P. Zawada, L.M. Butkus, G.A. Hartman, Tensile and fatigue behavior of silicon carbide fiber-reinforced aluminosilicate glass, J. Am. Ceram. Soc. 74 (11) (1991) 2851–2858.
[10] V.C. Nardone, K.M. Prewo, Tensile performance of carbon-fibre-reinforced glass, J. Mater. Sci. 23 (1) (1988) 168–180.
[11] M.S. Aly-Hassan, H. Hatta, S. Wakayama, M. Watanabe, K. Miyagawa, Comparison of 2D and 3D carbon/carbon composites with respect to damage and fracture resistance, Carbon 41 (5) (2003) 1069–1078.
[12] W. Huettner, Potential of carbon/carbon composites as structural materials, In: , Springer, 1990, pp. 275–300.
[13] T. Suzuki, T. Miyajima, M. Sakai, The role of the fiber/matrix interface in the first matrix cracking of fiber-reinforced brittle-matrix composites, Compos. Sci. Technol. 51 (2) (1994) 283–289.
[14] T. Miyajima, M. Sakai, Fiber bridging of a carbon fiber-reinforced carbon matrix lamina composite, J. Mater. Res. 6 (3) (1991) 539–547.
[15] L. Wei, S. Meng, C. Xu, F. Qi, X. Tian, Real-time observation of damage nucleation in three-dimensionally reinforced carbon/carbon composites and role of bundle/matrix interface, Adv. Compos. Mater. 22 (3) (2013) 165–174.
[16] O. Seh-Min, L. Jai-Young, Fracture behavior of two-dimensional carbon/carbon composites, Carbon 27 (3) (1989) 423–430.
[17] H. Mahfuz, M. Maniruzzaman, J. Krishnagopalan, A. Haque, M. Ismail, S. Jeelani, Effects of stress ratio on fatigue life of carbon-carbon composites, Theor. Appl. Fract. Mech. 24 (1) (1995) 21–31.
[18] L.-Z. Xue, K.-Z. Li, Y. Jia, S.-Y. Zhang, J. Cheng, J. Guo, Flexural fatigue behavior of 2D cross-ply carbon/carbon composites at room temperature, Mater. Sci. Eng. A 634 (2015) 209–214.
[19] X. Liao, H. Li, W. Xu, K. Li, Effects of tensile fatigue loads on flexural behavior of 3D braided C/C composites, Compos. Sci. Technol. 68 (2) (2008) 333–336.
[20] A. Ozturk, R.E. Moore, Tensile fatigue behaviour of tightly woven carbon/carbon composites, Composites 23 (1) (1992) 39–46.
[21] Y. Tanabe, T. Yoshimura, T. Watanabe, T. Hiraoka, Y. Ogita, E. Yasuda, Fatigue of C/C composites in bending and in shear modes, Carbon 42 (8 9) (2004) 1665–1670.
[22] K. Goto, H. Hatta, D. Katsu, T. Machida, Tensile fatigue of a laminated carbon--carbon composite at room temperature, Carbon 41 (6) (2003) 1249–1255.
[23] P. Chowdhury, H. Sehitoglu, R. Rateick, Damage tolerance of carbon-carbon composites in aerospace application, Carbon 126 (2018) 382–393.
[24] S. Ozcan, P. Filip, Wear of carbon fiber reinforced carbon matrix composites: study of abrasive, oxidative wear and influence of humidity, Carbon 62 (2013) 240–247.
[25] S. Yu, et al., Tribological properties of carbon/carbon composites with various pyrolytic carbon microstructures, Wear 304 (1 2) (2013) 103–108.
[26] D.-G. Kim, D.-W. Kweon, J.-Y. Lee, The wear properties of carbon/carbon composites prepared by chemical vapour deposition, J. Mater. Sci. Lett. 12 (1) (1993) 8–10.
[27] C. Blanco, J. Bermejo, H. Marsh, R. Menendez, Chemical and physical properties of carbon as related to brake performance, Wear 213 (1 2) (1997) 1–12.
[28] B.K. Yen, An investigation of friction and wear mechanisms of carbon-carbon composites in nitrogen and air at elevated temperatures, Carbon 34 (4) (1996) 489–498.
[29] S. Ozcan, P. Filip, Microstructure and wear mechanisms in C/C composites, Wear 259 (1 6) (2005) 642–650.
[30] K. Fujita, H. Sakai, N. Iwashita, Y. Sawada, Influence of heat treatment temperature on interfacial shear strength of C/C, Compos. Part A Appl. Sci. Manuf. 30 (4) (1999) 497–501.
[31] Y. Furukawa, H. Hatta, Y. Kogo, Interfacial shear strength of C/C composites, Carbon 41 (9) (2003) 1819–1826.
[32] H. Hatta, K. Goto, S. Ikegaki, I. Kawahara, M.S. Aly-Hassan, H. Hamada, Tensile strength and fiber/matrix interfacial properties of 2D-and 3D-carbon/carbon composites, J. Eur. Ceram. Soc. 25 (4) (2005) 535–542.
[33] M. Sakai, R. Matsuyama, T. Miyajima, The pull-out and failure of a fiber bundle in a carbon fiber reinforced carbon matrix composite, Carbon 38 (15) (2000) 2123–2131.
[34] J. Tezcan, S. Ozcan, B. Gurung, P. Filip, Measurement and analytical validation of interfacial bond strength of PAN-fiber-reinforced carbon matrix composites, J. Mater. Sci. 43 (5) (2008) 1612–1618.
[35] S. Ozcan, J. Tezcan, B. Gurung, P. Filip, The effect of heat treatment temperature on the interfacial shear strength of C/C composites, J. Mater. Sci. 46 (1) (2011) 38–46.
[36] P. Diss, J. Lamon, L. Carpentier, J.L. Loubet, P. Kapsa, Sharp indentation behavior of carbon/carbon composites and varieties of carbon, Carbon 40 (14) (2002) 2567–2579.
[37] D.T. Marx, L. Riester, Mechanical properties of carbon carbon composite components determined using nanoindentation, Carbon 37 (11) (1999) 1679–1684.
[38] T.S. Gross, N. Timoshchuk, I.I. Tsukrov, R. Piat, B. Reznik, On the ability of nanoindentation to measure anisotropic elastic constants of pyrolytic carbon, ZAMM-J. Appl. Math. Mech. für Angew. Math. und Mech. 93 (5) (2013) 301–312.
[39] S. Ozcan, J. Tezcan, P. Filip, Microstructure and elastic properties of individual components of C/C composites, Carbon 47 (15) (2009) 3403–3414.
[40] F. Tuinstra, J. Lo Koenig, Raman spectrum of graphite, J. Chem. Phys. 53 (3) (1970) 1126–1130.
[41] J.-M. Vallerot, X. Bourrat, A. Mouchon, G. Chollon, Quantitative structural and textural assessment of laminar pyrocarbons through Raman spectroscopy, electron diffraction and few other techniques, Carbon 44 (9) (2006) 1833–1844.
[42] M.R. Ammar, J.-N. Rouzaud, How to obtain a reliable structural characterization of polished graphitized carbons by Raman microspectroscopy, J. Raman Spectrosc. 43 (2) (2012) 207–211.
[43] A.C. Ferrari, J. Robertson, Interpretation of Raman spectra of disordered and amorphous carbon, Phys. Rev. B 61 (20) (2000) 14095.
[44] L. Nikiel, P.W. Jagodzinski, Raman spectroscopic characterization of graphites: a re-evaluation of spectra/structure correlation, Carbon 31 (8) (1993) 1313–1317.
[45] A. Cuesta, P. Dhamelincourt, J. Laureyns, A. Martinez-Alonso, J.M.D. Tascón, Raman microprobe studies on carbon materials, Carbon 32 (8) (1994) 1523–1532.
[46] P. Lespade, A. Marchand, M. Couzi, F. Cruege, Caracterisation de materiaux carbones par microspectrometrie Raman, Carbon 22 (4 5) (1984) 375–385.
[47] R.J. Nemanich, S.A. Solin, First-and second-order Raman scattering from finite-size crystals of graphite, Phys. Rev. B 20 (2) (1979) 392.
[48] W. Zhang, B. Reznik, O. Deutschmann, Raman microprobe spectrometry of carbon/carbon composites with differently-textured pyrolytic carbon matrices, ZAMM-J. Appl. Math. Mech. für Angew. Math. und Mech. 93 (5) (2013) 329–337.
[49] L.S. Schadler, C. Galiotis, Fundamentals and applications of micro Raman spectroscopy to strain measurements in fibre reinforced composites, Int. Mater. Rev. 40 (3) (1995) 116–134.
[50] R.J. Diefendorf, E.W. Tokarsky, The Relationship of Structure to Properties in Graphite Fibers. Part 1, 1971.
[51] P. Dupel, X. Bourrat, R. Pailler, Structure of pyrocarbon infiltrated by pulse-CVI, Carbon 33 (9) (1995) 1193–1204.
[52] X. Bourrat, F. Langlais, G. Chollon, G.L. Vignoles, Low temperature pyrocarbons: a review, J. Braz. Chem. Soc. 17 (6) (2006) 1090–1095.

[53] J.-M. Vallerot, X. Bourrat, Pyrocarbon optical properties in reflected light, Carbon 44 (8) (2006) 1565–1571.
[54] W. Kowbel, J. Don, TEM study of the microstructure of carbon-carbon composite, J. Mater. Sci. 24 (1) (1989) 133–138.
[55] S.C. Bennett, D.J. Johnson, Electron-microscope studies of structural heterogeneity in PAN-based carbon fibres, Carbon 17 (1) (1979) 25–39.
[56] B. Riccardi, R. Montanari, Indentation of metals by a flat-ended cylindrical punch, Mater. Sci. Eng. A 381 (1 2) (2004) 281–291.
[57] R.H. Telling, M.I. Heggie, Stacking fault and dislocation glide on the basal plane of graphite, Phil. Mag. Lett. 83 (7) (2003) 411–421.
[58] G.M. Jenkins, Basal plane distortion in pyrolytic carbon, Carbon 7 (1) (1969) 9–14.
[59] W. V Kotlensky, Analysis of high temperature creep in pyrolytic carbon, Carbon 4 (2) (1966) 209–214.
[60] R.E. Franklin, Crystallite growth in graphitizing and non-graphitizing carbons, Proc. Roy. Soc. Lond. A 209 (1097) (1951) 196–218.
[61] A.C. Fischer-Cripps, Nanoindentation, Springer, New York, 2004.
[62] W.C. Oliver, G.M. Pharr, An improved technique for determining hardness and elastic modulus using load and displacement sensing indentation experiments, J. Mater. Res. 7 (6) (1992) 1564–1583.
[63] T. Csanádi, D. Németh, C. Zhang, J. Dusza, Nanoindentation derived elastic constants of carbon fibres and their nanostructural based predictions, Carbon 119 (2017) 314–325.
[64] H. Miyagawa, T. Mase, C. Sato, E. Drown, L.T. Drzal, K. Ikegami, Comparison of experimental and theoretical transverse elastic modulus of carbon fibers, Carbon 44 (10) (2006) 2002–2008.
[65] R. Maurin, P. Davies, N. Baral, C. Baley, Transverse properties of carbon fibres by nano-indentation and micro-mechanics, Appl. Compos. Mater. 15 (2) (2008) 61.
[66] R.F. Gibson, A review of recent research on nanoindentation of polymer composites and their constituents, Compos. Sci. Technol. 105 (2014) 51–65.
[67] Y. Sun, G. Zhao, F. Yang, Anisotropic behavior of the nanoindentation of single carbon fibers, Nanosci. Nanotechnol. Lett. 6 (7) (2014) 596–600.
[68] A. Oberlin, P.A. Thrower, Chemistry and Physics of Carbon, vol. 22, Marcel Dekker, New York, 19891–143.
[69] R.E. Franklin, The structure of graphitic carbons, Acta Crystallogr. 4 (3) (1951) 253–261.
[70] D. Nečas, P. Klapetek, Gwyddion: an open-source software for SPM data analysis, Open Phys. 10 (1) (2012) 181–188.
[71] Z.-H. Xu, X. Li, Effect of sample tilt on nanoindentation behaviour of materials, Philos. Mag. A 87 (16) (2007) 2299–2312.
[72] X. Bourrat, A. Fillion, R. Naslain, G. Chollon, M. Brendlé, Regenerative laminar pyrocarbon, Carbon 40 (15) (2002) 2931–2945.
[73] M. Shioya, E. Hayakawa, A. Takaku, Non-hookean stress-strain response and changes in crystallite orientation of carbon fibres, J. Mater. Sci. 31 (17) (1996) 4521–4532.
[74] C. Sauder, J. Lamon, R. Pailler, The tensile behavior of carbon fibers at high temperatures up to 2400 C, Carbon 42 (4) (2004) 715–725.
[75] H. Rennhofer, D. Loidl, S. Puchegger, H. Peterlik, Structural development of PAN-based carbon fibers studied by in situ X-ray scattering at high temperatures under load, Carbon 48 (4) (2010) 964–971.
[76] T. Noda, K. Kamiya, M. Inagaki, Effect of pressure on graphitization of carbon. I. Heat treatment of soft carbon under 1, 3 and 5 kbar, Bull. Chem. Soc. Jpn. 41 (2) (1968) 485–492.
[77] R.J. Zaldivar, G.S. Rellick, Some observations on stress graphitization in carbon-carbon composites, Carbon 29 (8) (1991) 1155–1163.
[78] R.B. Mathur, O.P. Bahl, T.L. Dhami, S.K. Chauhan, A novel route to realise high degree of graphitization in carbon-carbon composites derived from hard carbons, Carbon Lett. 4 (3) (2003) 111–116.
[79] F. Zhang, B. Huang, Q. Huang, X. Xiong, T. Cheng, Effects of the interface on the graphitization of a carbon fiber/pyrolytic carbon composite, Carbon 3 (41) (2003) 610–612.
[80] L.J. Lanticse-Diaz, Y. Tanabe, T. Enami, K. Nakamura, M. Endo, E. Yasuda, The effect of nanotube alignment on stress graphitization of carbon/carbon nanotube composites, Carbon 47 (4) (2009) 974–980.
[81] K. Matsui, L.J. Lanticse, Y. Tanabe, E. Yasuda, M. Endo, Stress graphitization of C/C composite reinforced by carbon nanofiber, Carbon 7 (43) (2005) 1577–1579.
[82] Y. Hishiyama, M. Inagaki, S. Kimura, And others, Graphitization of carbon fibre/glassy carbon composites, Carbon 12 (3) (1974) 249–258.
[83] G.S. Rellick, D.J. Chang, R.J. Zaldivar, Mechanisms of orientation and graphitization of hard-carbon matrices in carbon/carbon composites, J. Mater. Res. 7 (10) (1992) 2798–2809.
[84] J.-M. Leyssale, J.-P. Da Costa, C. Germain, P. Weisbecker, G.L. Vignoles, Structural features of pyrocarbon atomistic models constructed from transmission electron microscopy images, Carbon 50 (12) (2012) 4388–4400.
[85] S. Plimpton, Fast parallel algorithms for short-range molecular dynamics, J. Comput. Phys. 117 (1) (1995) 1–19.
[86] J. Tersoff, Empirical interatomic potential for carbon, with applications to amorphous carbon, Phys. Rev. Lett. 61 (25) (1988) 2879.
[87] J.H. Los, A. Fasolino, Intrinsic long-range bond-order potential for carbon: performance in Monte Carlo simulations of graphitization, Phys. Rev. B 68 (2) (2003) 24107.
[88] S.J. Stuart, A.B. Tutein, J.A. Harrison, A reactive potential for hydrocarbons with intermolecular interactions, J. Chem. Phys. 112 (14) (2000) 6472–6486.
[89] J. Hafner, Ab-initio simulations of materials using VASP: density-functional theory and beyond, J. Comput. Chem. 29 (13) (2008) 2044–2078.